ARTICLES

Femtosecond Pump−Probe Transient Absorption Study of the Photolysis of $[Cp'Mo(CO)_3]_2$ ($Cp' = \eta^5$-$C_5H_4CH_3$): Role of Translational and Rotational Diffusion in the Radical Cage Effect

Alan B. Oelkers, Lawrence F. Scatena, and David R. Tyler*

Department of Chemistry, University of Oregon, Eugene, Oregon 97403

Received: July 28, 2006; In Final Form: April 11, 2007

Femtosecond pump−probe studies of the photodissociation and subsequent radical cage pair recombination dynamics of the organometallic dimer $[Cp'Mo(CO)_3]_2$ ($Cp' = \eta^5$-$C_5H_4CH_3$) are reported. The dynamics following photodissociation were studied in numerous noncoordinating hydrocarbon solvents. The results indicate that primary geminate recombination occurs on an ultrafast time scale ($\tau \approx 5$ ps) and the efficiency of cage escape is inversely proportional to solvent viscosity. Investigation of the time-dependent anisotropy in this system allowed for an estimate of the rotational correlation time of the radical fragments ($\tau \approx 5-25$ ps). Comparison of the rates of rotational motion with the population kinetics shows that the primary solvent cage dynamics and recombination efficiency are controlled by radical diffusion and not by radical rotation.

Introduction

In liquid-phase chemical reactions, the solvent plays a prominent role in controlling the reactivity between potential reaction partners. A notable demonstration of this is seen in photodissociation reactions, where the surrounding solvent may cause primary photoproducts to remain in close proximity for a finite period following dissociation, potentially leading to recombination of the newly formed fragments. This phenomenon, termed the solvent cage effect, can reduce the quantum yield of photolysis and may often determine the ultimate fate of photochemical and thermal reactions.[1] Since the early work of Franck and Rabinowitch, the photodissociation of I_2 has served as a prototypical system to study the cage effect phenomenon.[2] Considerable insight into solvent caging was provided by the early experimental and theoretical work of Noyes and co-workers, whose results generated an increased interest in solvent cage reactions.[3−9] These early investigations relied on the use of various indirect photochemical techniques in order to measure an ultrafast process that is normally hidden from traditional kinetic observations.

Reasonably, I_2 has been the most studied subject in ultrafast investigations of the solvent cage effect. The weight of evidence from ultrafast studies of I_2 and from fundamental studies of the geminate recombination of similar small molecules has supported certain conclusions about the dynamics of geminate recombination in such systems: notably, that the primary cage lifetime is very short ($\tau_{cage} \approx$ few picoseconds) and that the recombination probability is largely controlled by the solvent properties (i.e., density and viscosity).[10−15]

Although the conclusions about the dynamics of solvent caging gained from research on I_2 and other small molecules are well supported, it is not clear that such behavior is universal, considering that these results represent systems in which the fragments have essentially no orientational restrictions for recombination. Femtosecond resolution studies of larger, polyatomic molecules, which do have orientational restrictions for recombination, are noticeably less common in the literature. Some relevant examples include the picosecond[16,17] and femtosecond[18] direct kinetic studies of azo compounds in solution. However, azo compounds are nonideal probes of primary geminate caging kinetics because the photodissociation reaction extrudes a molecule of N_2 between the nascent reactive radical fragments, leading to an initially separated radical pair. The photodissociation of disulfide complexes, which photolyze directly to form two symmetric radical pairs, has also been investigated as a probe of the solvent cage effect in larger organic molecules. Early picosecond studies showed the predicted relationship between solvent viscosity and caging efficiency in disulfides,[19] but the 35 ps resolution of the experiment was insufficiently fast to resolve the earliest-time events that have been shown to dominate the caging dynamics of small molecules. Ernsting and co-workers studied several disulfide systems with femtosecond resolution and observed ultrafast, direct generation of the radical fragments, which were shown to cage on a picosecond time scale, and they presented evidence of competition between solvation and geminate recombination within this time frame.[20,21]

Interest in solvent cage reactions of larger molecules has recently become a topic of some interest due to the potential for stereochemical control of certain organic transformations in confined media and the possibility of exploiting solvent caging to control carbon−carbon bond formation in supramolecular systems.[22−25] Because the ultrafast dynamics of solvent caging in such systems is still relatively unexplored, further research is needed to answer several fundamental questions about geminate recombination in large molecules that have

* Corresponding author. E-mail: dtyler@uoregon.edu.

10.1021/jp064849z CCC: $37.00
Published on Web 06/07/2007

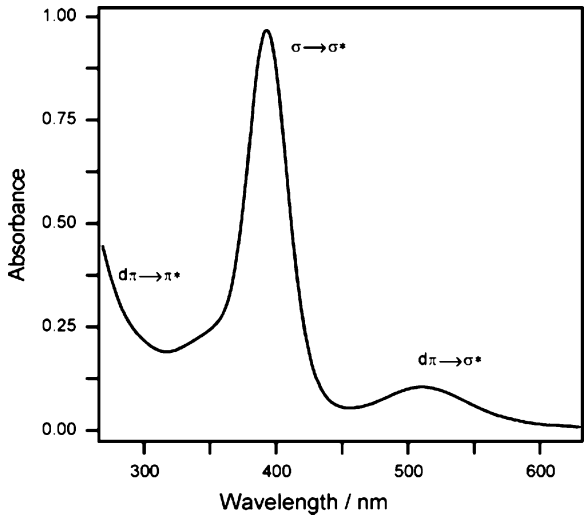

Figure 1. Electronic absorption spectrum of $[Cp'Mo(CO)_3]_2$. The annotations show the transition assignments of the absorption bands.

orientational restrictions for recombination. Of particular interest is whether geminate recombination is controlled by the escape efficiency during a short picosecond encounter period or rather if the dynamics can be described best by a relatively long-lived encounter period where the recombination efficiency is controlled by proper alignment of the fragments. In this paper we present a study of the dynamics of geminate recombination of an organometallic molecule, $[Cp'Mo(CO)_3]_2$ ($Cp' = \eta^5$-$C_5H_4CH_3$), based on femtosecond visible pump−probe time-resolved kinetic population data and time-resolved anisotropy data.

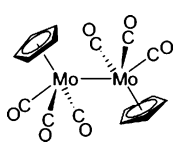

Metal−metal bonded carbonyl compounds are an excellent system for the study of ultrafast photochemical reactions because the metal−metal bond is, in many cases, an example of an ideal photolabile bond.[26] The $[Cp'Mo(CO)_3]_2$ complex is a well-studied example of such a compound. The electronic absorption spectrum of the complex displays two prominent absorption peaks in the visible: a sharp, intense band with λ_{max} at 390 nm and a less intense, broad peak with λ_{max} at 515 nm (Figure 1).

The generally accepted interpretation of the electronic structure and absorption spectra in this system was provided originally by Wrighton and Ginley,[27] who assigned the intense 390 nm band as a $\sigma \rightarrow \sigma^*$ transition and the less intense band at 515 nm to a $d\pi \rightarrow \sigma^*$ transition. Both visible transitions are localized to the metal−metal bond. Comprehensive experimental evidence revealed that irradiation into the $d\pi \rightarrow \sigma^*$ band leads exclusively to homolytic cleavage of the metal−metal bond, generating a pair of 17-electron radicals, while irradiation into the $\sigma \rightarrow \sigma^*$ band produces both homolytic cleavage of the metal bond and carbonyl dissociation products.[27−29] The latter result is most likely a consequence of the overlap of the higher energy $d\pi \rightarrow \pi^*$ (CO) metal-to-ligand charge transfer band (MLCT) with the $\sigma \rightarrow \sigma^*$ band.[30]

Because of the well-described and predictable photochemistry of this compound, the system is ideally suited to a two-color visible pump−probe experiment whereby geminate radical pairs are generated by M−M bond photolysis (515 nm) and reaction

SCHEME 1

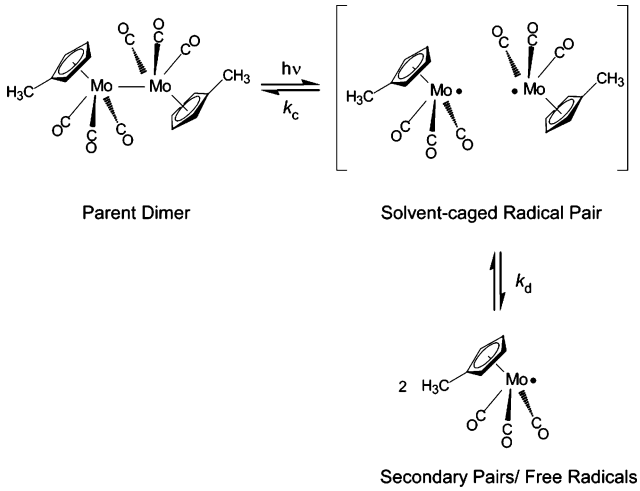

progress may be followed by monitoring a visible (400 nm) parent absorption band (Scheme 1).[27,29]

Several earlier studies investigated the kinetics of radical self-termination in this system with flash photolysis,[31,32] nanosecond visible pump−probe spectroscopy,[33] and nanosecond resolution infrared studies.[34] These studies demonstrated that visible irradiation ($d\pi \rightarrow \sigma^*$) leads to efficient metal−metal bond photolysis, and they provided accurate estimations of the rate constants for the diffusion-limited bimolecular free-radical self-termination reaction (k_{Mo-Mo} ca. $(3-4) \times 10^9$ M^{-1} s^{-1}; hexane or CH_3CN)[31,33] and the gauche−trans isomerization of the parent dimer (k_{g-t} ca. 1×10^3 s^{-1}).[34] Several published investigations of the photochemistry of $[CpMo(CO)_3]_2$ in frozen matrixes have demonstrated that no new absorption bands appear in the visible spectrum following visible ($\lambda > 400$ nm) irradiation, while the metastable CO-loss intermediate is shown to have a new absorption band only in the UV ($\lambda_{max} = 330$ nm).[35−38] In other work, ultrafast research with $M_2(CO)_{10}$ (M = Mn, Re) demonstrated homolytic metal−metal bond dissociation on an ultrafast time scale, generating symmetric 17-electron radicals.[39−42] Given the similar orbital parentage, electronic structure, band structure, and observed photochemistry of these systems to the Cp substituted group VI dimer,[28] the $[Cp'Mo(CO)_3]_2$ system seemed an ideal platform for studying solvent cage effects. We describe here the utilization of this system in exploring a fundamental picture of geminate recombination dynamics in large, anisotropic molecules.

Methods

Samples. $[Cp'Mo(CO)_3]_2$ was synthesized according to standard literature methods.[43] The air- and light-sensitive samples were handled under an N_2 atmosphere in a dark glovebox or on a Schlenk line using standard anaerobic techniques. The solvents used in the photolysis studies were obtained from Aldrich and were dried through appropriate methods and rigorously deoxygenated by purging with N_2 or argon prior to photolysis studies. The solutions subjected to pump−probe studies were deposited into a custom-built vacuum-tight fluid reservoir/recirculating flow cell system and blanketed under an atmosphere of dry N_2. The concentrations of the prepared solutions were all approximately 1 mM. This concentration was chosen in order to have an optical density of approximately 0.5−1.0 at 400 nm in the flow cell (path length = 500 μM). The integrity of the solutions was confirmed after the completion of spectroscopic measurements by collection of the UV−visible spectra of the solutions.

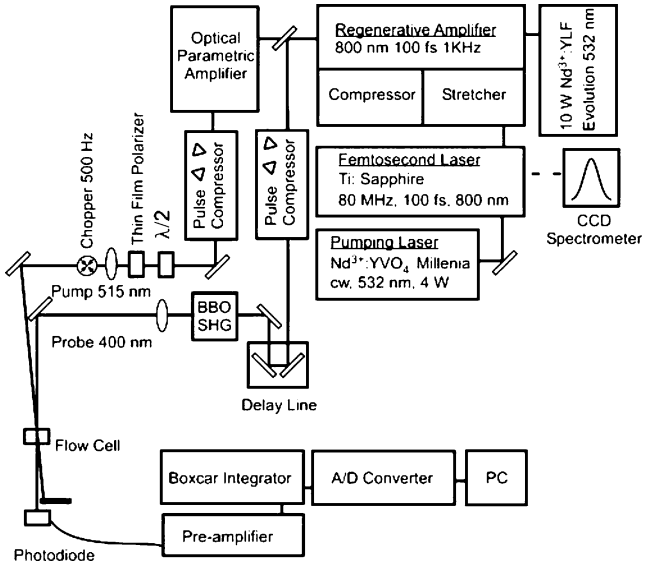

Figure 2. Femtosecond laser system.

Femtosecond Laser System. The studies of solvent caging were carried out using the femtosecond laser system described below. The source is a home-built, Kerr-lens passively mode-locked Ti:sapphire laser, pumped by a solid-state intracavity-doubled 532 nm continuous wave 5 W Nd:YVO_4 laser (Spectra-Physics Millenia). The oscillator output seeds a stretched-chirped pulse regenerative amplifier (Spectra-Physics Spitfire) pumped by an 8 W intracavity-doubled 1 kHz Nd:YLF laser (Spectra-Physics Evolution). The amplifier output is a 1 kHz pulse train of 100 fs pulses with wavelength centered at 800 nm. The two-color pump−probe experiments were carried out using a pump wavelength of 515 nm created by optical parametric amplification of the 800 nm amplifier output (Spectra-Physics OPA 800-C) and a probe wavelength of 400 nm generated as the second harmonic of the amplifier output using a type I β-barium borate (BBO) crystal.

Optical Layout. The pump and probe beams are subjected to a paired-prism compressor in order to maintain the minimum time−bandwidth product at the sample interface.[44] The added path delay is introduced by a mechanical linear translation stage (Aerotech ATS-2060). The pump signal is modulated to 500 Hz, or half the rate of the probe pulse with a mechanical chopper. The probe signal is detected using a biased silicon photodiode (Thorlabs DET 210), amplified with a fast preamplifier (SRS-SR445A) and sampled with a boxcar integrator (SRS-SR250). The boxcar output is connected to an analog-to-digital converter and a PC. The air-sensitive samples were studied using a custom-built anaerobic flow cell equipped with 1 mm thick CaF_2 windows and a 500 μm path length. CaF_2 was used as the window material due to its low dispersion at the wavelengths used and chemical inertness to the reaction mixtures. Determination of the pump−probe cross-correlation was achieved by measuring a nonlinear artifact at the sample interface.[45,46] The energies of the pump and probe pulses at the flow cell interface were approximately 8 and 0.5 μJ, respectively. The signal response at short times was found to be linear with pump power, indicating a linear photoprocess. Three polarization schemes were used in these measurements. A "magic-angle" configuration of 54.7° between the plane-polarized pump and probe beams was used to collect isotropic data in order to determine population specific kinetics, and perpendicular and parallel orientations were used to calculate the time-dependent anisotropy of the sample.

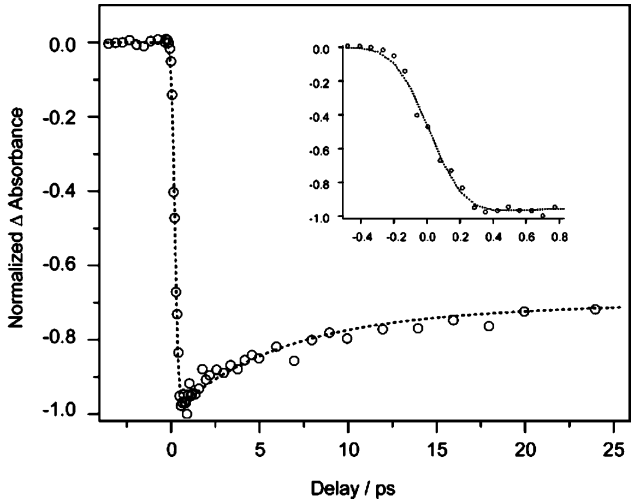

Figure 3. Transient-absorption kinetic data of $[Cp'Mo(CO)_3]_2$ (approximately 1 mM) in neat cyclohexane monitored at 400 nm following photolysis at 515 nm displaying transient bleach and partial recovery of the parent signal within the first 25 ps. The inset displays the same data within ca. 1 ps, demonstrating the approximately 200 fs transient-bleach onset dictated by the instrument response function (IRF). The dashed line represents an empirical fit of the data to two exponential rise-to-max functions convoluted with the IRF (see text).

Results and Discussion

Femtosecond Transient-Absorption of $[Cp'Mo(CO)_3]_2$. Figure 3 shows the time-resolved pump−probe kinetic data of $[Cp'Mo(CO)_3]_2$ photolysis in cyclohexane. The kinetic trace was generated from a two-color femtosecond pump−probe transient-absorption experiment with a pump wavelength of 515 nm, corresponding to the d$\pi \rightarrow \sigma^*$ transition of the molecule, and probed at 400 nm, corresponding to the most intense absorption band of the parent dimer ($\sigma \rightarrow \sigma^*$). (The data were collected with a magic-angle (54.7°) polarization orientation between the plane-polarized pump and probe pulse trains.) The data are thus a measurement of the parent dimer population kinetics.

Satisfactory fits to the entire kinetic trace were achieved by fitting the data to a biexponential equation that included two exponential rise-to-max functions and a nondecaying component convoluted with the instrument response function (eq 1).

$$\Delta A = [A_1(1 - \exp(-t/\tau_1)) + A_2(1 - \exp(-t/\tau_2)) + A_3](\mathrm{IRF}) \quad (1)$$

In this equation, ΔA represents the time-dependent transient absorption of the sample, A_1 and A_2 are the preexponential factors of the two processes, A_3 is the amplitude of the nondecaying component, τ_1 and τ_2 are the time constants ($\tau = k^{-1}$), and IRF represents the instrument response function.

The IRF (eq 2) represents the instrument-limited time resolution of the measurement, assuming a Gaussian temporal profile. In this equation, "erf" represents the error function and

$$\mathrm{IRF} = \frac{1}{2}\left[1 + \mathrm{erf}\left(\frac{t - \Delta t}{1.414\sigma}\right)\right] \quad (2)$$

the width parameter (σ) is taken from the prior measurement of the pump−probe cross-correlation. The cross-correlation measurements were fit to a temporal full width at half-maximum (fwhm) of approximately 200 fs, establishing the minimum temporal resolution for the pump−probe studies. For all samples investigated, the residual plots revealed no consistent bias.

Fitting the measured kinetic traces obtained in straight-chain alkane solvents revealed two prominent parent bleach recovery

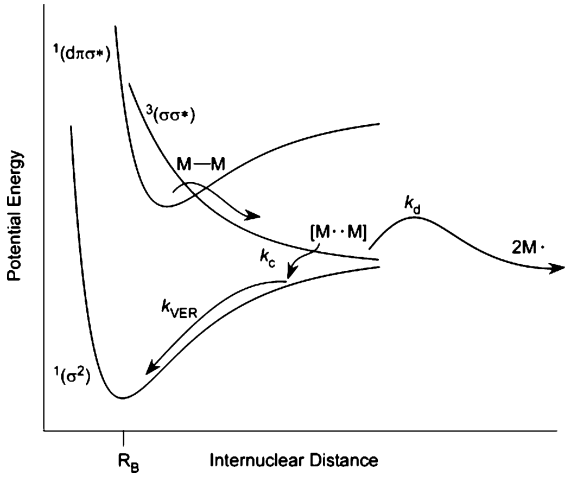

Figure 4. Proposed mechanism of the photodissociation and ultrafast reaction dynamics of $[Cp'Mo(CO)_3]_2$ following irradiation at 515 nm. The rate constants in the figure are related to the empirically measured rate constants by $k_1 = \tau_1^{-1} = (k_c + k_d)$ and the observed vibrational relaxation time $\tau_2 = k_{VER}^{-1}$ (see text). The k_d diffusion barrier for the radical caged pair represents the intercalation of a solvent molecule between the geminate radicals.

rates with time constants ($\tau = k^{-1}$) of approximately 5 ps (τ_1) and 80 ps (τ_2). The chemical interpretation of these processes is aided by an understanding of the photochemistry of this system and by the solvent studies explained below. Collectively, this information leads us to tentatively propose the following kinetic model. The observed data are consistent with an ultrafast photodissociation of the Mo−Mo bond following irradiation at 515 nm to form a short-lived primary radical cage pair with a lifetime of about 5 ps. It is suggested that the slower rate ($\tau_2 \geq$ 70 ps) is the subsequent vibrational energy relaxation (VER) of the newly re-formed parent dimer following recombination of the geminate cage pair. The model is shown in Figure 4.

Because the kinetic model describes the radical caged pair as being affected by a pair of competitive first-order reactions, the intrinsic rate constants controlling geminate recombination, k_c and k_d, may be readily extracted from the empirically measured kinetic data by applying the expression for the competition of two first-order rates (eq 3).

$$[M{-}M]_t = \left(\frac{k_c}{k_c + k_d}\right)[M^{\bullet},{}^{\bullet}M]_0(1 - e^{-((k_c+k_d)t)}) \qquad (3)$$

Thus, the empirically measured τ_1 is related to the rate constants for recombination (k_c) and cage escape (k_d) by the following:

$$\tau_1^{-1} = k_1 = (k_c + k_d) \qquad (4)$$

In this model, the bleach recovery of the parent signal at 400 nm following photolysis at 515 nm is attributed solely to repopulation of the ground electronic/vibrational state of the parent dimer following geminate recombination. Thus, the cage efficiency factor (F_c), or total fraction caged by the solvent, may be obtained from the kinetic trace fit amplitudes. From these kinetic data, F_c is conceptually identified with the absorbance of the bleach recovery plateau when these are the only competing processes. The extraction of F_c from these data is shown here based on the variables extracted from the empirical fit (eq 5).

$$F_c = \frac{k_c}{k_c + k_d} = -\left(\frac{A_1 + A_2}{A_3}\right) \qquad (5)$$

Using the empirical measurement of F_c, the values of k_c and k_d may be determined individually by rearranging eqs 4 and 5 (eq 6).

$$k_c = F_c(k_c + k_d) = F_c(k_1) \qquad (6)$$

To gain further insight into the dynamics following photolysis, the femtosecond kinetics of the $[Cp'Mo(CO)_3]_2$ system were studied in numerous solvents with different physical properties. A summary of the results is shown in Table 1.

Inspection of the solvent dependence of the kinetic data reveals trends that are consistent with the proposed kinetic model. Most significant is the direct correlation of both τ_1 and F_c with solvent viscosity. Furthermore, a comparison of k_c and k_d with solvent viscosity (η) reveals no identifiable solvent dependence of k_c, but a strong correlation with k_d. The linear relationship between k_d and $1/\eta$ (Figure 5) is evidence supporting a diffusion-controlled process as predicted by the Stokes−Einstein−Smoluchowski equation.[47]

The solvents used for comparison in this study included straight-chain alkanes, cycloalkanes, 1-propanol, and squalane, a 30-carbon alkane with methyl side chains. The observation that geminate recombination is controlled by the diffusion rate constant (k_d) (which is proportional to bulk solvent viscosity) supports the conclusion that solvent viscosity is a suitable parameter to describe the efficiency of geminate recombination in this system. These results, which demonstrate a strong correlation between both k_d and the caging efficiency (F_c) with solvent viscosity, are consistent with most previous investigations of the cage effect in which solvent viscosity was explicitly studied. From such studies, most evidence suggests that solvent viscosity is the only solvent parameter which can reliably be expected to correlate with F_c.[48−52] These results seem to further support the consensus on this issue.

In contrast, the relationship between the slower process (τ_2) and the solvent identity is more complicated, but the results are consistent with the attribution of this process to vibrational energy relaxation (VER) of the newly re-formed parent dimer. Inspection of the solvent dependence of τ_2 shows a correlation both to solvent viscosity and to the solvent type. Looking specifically at solvent type, it is noted that the τ_2 values in *n*-alkanes are all approximately 80 ps, which is clearly distinct from the τ_2 values in cycloalkane solvents (ca. 190 ps) and for the alcohol solvent, 1-propanol (ca. 400 ps). As explained next, these results suggest a solvent dependence that is consistent with VER.

For diatomic molecules, VER is a process that can be considerably long in weakly interacting systems, and the rate is dependent on the interaction of solute and solvent. In contrast, the rate of VER for a polyatomic molecule in solution depends upon the pathway, which can generally be either energy transfer to internal modes via intramolecular vibrational relaxation (IVR) or energy transfer to bath modes through external vibrational energy relaxation (EVR).[53] It is often assumed that VER for large polyatomics is rapid because of the large density of states available for IVR; however, this supposition is based on the assumption that sufficient coupling exists between the internal modes, which is often not the case. In experiments such as this where the vibrationally excited molecule studied is initially formed near the dissociation limit, the large amount of excess

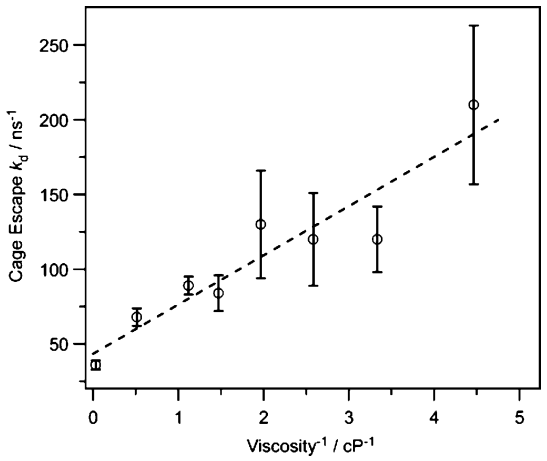

Figure 5. Comparison of rate constants for cage escape (k_d) vs solvent viscosity^{-1} (η^{-1}). The dashed line represents a linear fit to the data. A linear relationship between k_d and η^{-1} is evidence supporting a diffusion-controlled process. The error bars represent ± 1 standard deviation (σ) determined by propagating the uncertainty from the nonlinear least-squares regression fit of the kinetic traces (eq 1).

vibrational energy may have to escape an EVR bottleneck even when IVR is otherwise fast.

Existing experimental evidence of the VER time scale in metal carbonyls suggests rates with time constants of approximately tens to hundreds of picoseconds. For example, Joly and Nelson reported ca. 50 ps relaxation times for $M(CO)_6$ (M = Mo, Cr, W) from ultrafast transient absorption data,[54] Zhang and Harris reported two VER rates for $Mn_2(CO)_9$ of approximately 15 and 150 ps from ultrafast transient absorption studies,[26] and Steinhurst et al. performed UV-pump transient-IR probe spectroscopic studies of $Mn_2(CO)_{10}$ and determined VER cooling rates for the low-frequency modes of the nascent $Mn_2(CO)_9$ through transient line width narrowing methods, yielding estimated VER rates of approximately 60 ps.[55] Using similar methodology, Heilweil and co-workers reported a VER lifetime of 30 ps in $[CpFe(CO)_2]_2$.[56]

In the case of $[Cp'Mo(CO)_3]_2$, the Mo−Mo stretching mode is a very low frequency vibration (ca. 100 cm^{-1}) because the vibrational mode is one with heavy groups connected by a weak bond (ca. 35 kcal mol^{-1}). Low frequency vibrational modes such as this have energy spacings close to k_BT at room temperature and, hence, are usually considered to behave classically.[53] Inspection of the complete vibrational spectrum of $[Cp'Mo(CO)_3]_2$ reveals that there are no other modes of similar frequency, making EVR plausible as the main mechanism of vibrational cooling. Thus, for this molecule, the vibrational cooling rate may show solvent dependence because the bath modes should exist as the main sink for vibrational cooling of the dimer. In this respect, the vibrational relaxation of $[Cp'Mo(CO)_3]_2$ may resemble the mechanism of vibrational relaxation in I_2, a well-studied system with a fundamental stretch frequency of 215 cm^{-1} and reported solvent-dependent vibrational relaxation times of about 50−200 ps.[57] It should be noted, however, that it is difficult to describe the mechanism of VER in polyatomics, especially with respect to solvent trends, considering the pathways available involving the solvent (e.g., EVR or solvent-assisted IVR). These results do demonstrate a considerably slower VER rate in 1-propanol, a strong hydrogen-bonding solvent, in comparison to the alkane solvents studied, a result that is somewhat anomalous in comparison to earlier reported VER rates in metal carbonyls. Some of the studies mentioned above also investigated VER rates in both alkane and alcoholic solvents. For example, Zhang and Harris's similar experiment investigating the VER rate of nascent $Mn_2(CO)_9$ following the UV photolysis of $Mn_2(CO)_{10}$ demonstrated the opposite solvent trend: the two VER rates reported (approximately 10 and 150 ps) were assigned as a fast relaxation of the high-frequency CO stretch modes by IVR and slower relaxation of low-frequency modes, respectively; both rates were faster by 20−30% in 2-propanol vs cyclohexane.[26] Owrutsky and co-workers measured the VER rate of the same species ($Mn_2(CO)_9$) and reported VER rates of 45 ± 17 ps in cyclohexane vs 72 ± 35 ps in 2-propanol, results that are equivalent within one standard deviation.[55] Many other reported studies of VER in polyatomics show no specific solvent polarity trends even while other solvent parameters may influence the VER rate, for example in the VER studies of azulene.[58] Because it is difficult to unambiguously assign electronic transients, it is impossible to rule out the possibility that the slow process (τ_2) may include some contributions from secondary geminate recombination. Nevertheless, the collective kinetic and solvent-dependence data are consistent with the attribution of τ_2 to VER of the newly re-formed parent dimer.

A similar investigation into the dynamics of solvent caging using metal carbonyls was conducted by Harris and co-workers.[42] In this study, the events following absorption of 295 nm light in $Re_2(CO)_{10}$ were followed with 300 fs time resolution. Although both CO dissociation ($Re_2(CO)_9$) and Re−Re bond homolysis ($Re(CO)_5$) products were generated following UV excitation, the dynamics of both species were followed independently by monitoring the transient infrared spectra in the CO stretch region. With respect to the geminate recombination of the $Re(CO)_5$ radicals, recombination on 50 and 500 ps time scales was reported. The geminate recombination dynamics were described by fitting the observed transients to an equation based on a Smoluchowski-type diffusion model, which neglects the molecular properties of the solvent by treating it as a viscous continuum. In contrast to these findings, our results suggest faster recombination times in $Cp'Mo(CO)_3$ caged pairs. Although the solvent-dependent data reported in our study demonstrate a certain solvent viscosity correlation, the geminate recombination dynamics do not fit to a Smoluchowski-type diffusion equation.

Rotational Relaxation and Geminate Recombination of $[Cp'Mo(CO)_3]_2$. To gain greater insight into the dynamics of geminate recombination in this system, the ultrafast time-dependent anisotropy of $[Cp'Mo(CO)_3]_2$ was investigated. The time scale and solvent dependence of the rotational motion can be compared to the rates extracted from the population-specific (magic-angle) measurements in order to determine if the results represent a slow or rapid rotation regime. Empirical measurement of the time-dependent anisotropy was carried out by collecting the transient signals obtained from both parallel ($\Delta A_{\parallel}$) and perpendicular ($\Delta A_{\perp}$) relative orientations of the plane-polarized pump and probe pulses. With this information, it waspossible to calculate the time-dependent anisotropy, $r(t)$, using eq 7.

$$r(t) = \frac{\Delta A_{\parallel} - \Delta A_{\perp}}{\Delta A_{\parallel} + 2\Delta A_{\perp}} = \frac{2}{5}\langle P_2 \cos \theta(t)\rangle \qquad (7)$$

In this equation, $\theta(t)$ is the orientational relaxation of the chromophoric axis within time t, P_2 is the second Legendre polynomial, and the brackets $\langle\ \rangle$ define the ensemble average. It follows that the rigid limit of the anisotropy function is defined as 2/5 at $t = 0$ in the case where the pump and probe pulses are both interacting with the same transition dipole moment or

TABLE 1: Time Constants ($\tau = k^{-1}$), Cage Effect (F_c), and Solvent Viscosity from the Femtosecond Photolysis Kinetics of $[Cp'Mo(CO)_3]_2$

solvent	viscosity/cP	τ_1/ps	τ_2/ps	F_c	$k_c/10^{10}$ s^{-1}	$k_d/10^{10}$ s^{-1}
pentane	0.22	3.5 ± 0.5	70 ± 25	0.26 ± 0.05	7.5 ± 2.5	21 ± 7
hexane	0.30	5.6 ± 1.0	75 ± 15	0.32 ± 0.03	5.5 ± 1	12 ± 2
heptane	0.39	5.7 ± 1.3	90 ± 30	0.32 ± 0.04	5.5 ± 1.5	12 ± 3
octane	0.51	5.2 ± 1.4	90 ± 30	0.33 ± 0.04	6 ± 2	13 ± 4
methylcyclohexane	0.68	7.2 ± 1.0	190 ± 60	0.40 ± 0.04	5.5 ± 0.8	8 ± 1
cyclohexane	0.89	5.9 ± 0.4	190 ± 20	0.48 ± 0.01	8.1 ± 0.6	8.9 ± 0.6
1-propanol	1.95	8.0 ± 0.7	400 ± 70	0.45 ± 0.01	5.6 ± 0.5	6.8 ± 0.6
squalane	30	7.4 ± 0.6	210 ± 10	0.73 ± 0.01	9.9 ± 0.8	3.6 ± 0.3

where the transition dipole moments are parallel. The time-dependent anisotropy of $[Cp'Mo(CO)_3]_2$ was measured for all of the solvents in the preceding section. An example of the time-dependent anisotropy is shown in Figure 6.

In all of the solvents studied, the measured anisotropy was found to fit well to a first-order function (eq 8). In $[Cp'Mo(CO)_3]_2$, both pump ($\lambda_{pump} = 515$ nm) and probe ($\lambda_{probe} = 400$) pulses interact with transitions localized to the Mo−Mo bond,

$$r(t) = \frac{2}{5}\exp(-t/\tau_R) \tag{8}$$

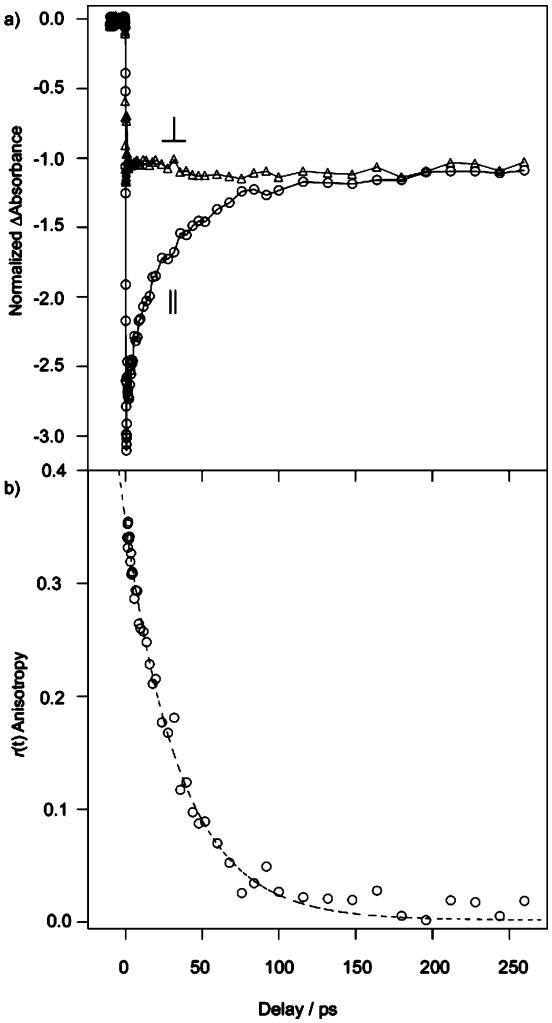

Figure 6. (a) Normalized differential absorption of pump-induced parallel (○) and perpendicular (△) polarization schemes of $[Cp'Mo(CO)_3]_2$ in cyclohexane detected with a $\lambda_{probe} = 400$ nm pulse following photolysis at 515 nm. The traces were normalized by tail-matching at 2−4 ns delay. (b) Time-dependent parent bleach anisotropy calculated from the perpendicular and parallel traces using eq 7. The line represents a first-order fit to the data (see text).

and hence the observed anisotropy is a measurement of the rotational relaxation rate of this chromophore. This measurement is not complicated by the simultaneous radical self-annihilation (geminate recombination), as there are no laboratory-frame orientational restrictions on the recombination event. The long-lived transient bleach caused by bond photodissociation allows for the anisotropy measurement by transient absorption, which is conceptually very similar to a fluorescence anisotropy measurement.

Normally, an observation of first-order decay of the time-dependent anisotropy from the rigid limit of 2/5 at $t = 0$ to an isotropically averaged value of 0 is taken as evidence of random relaxation of a spherically shaped solute.[59] However, the same behavior may result from the relaxation of an ellipsoidal solute when the main symmetry axis and transition dipole moment are aligned. To a close approximation, the shape of *anti*-$[Cp'Mo(CO)_3]_2$ is a prolate ellipsoid in which the chromophore axis is nearly collinear with the main symmetry axis. (Note that *anti*-$[Cp'Mo(CO)_3]_2$ is the most stable conformation in most solvents.[60,61]) The anisotropy equation for a prolate ellipsoid with aligned symmetry and chromophoric axes depends only on the diffusion coefficient perpendicular to the main symmetry axis, the generalized solution of which is essentially identical to the formulation for a spherical particle (eq 9).[59] (The term,

$$r(t) = \frac{2}{5}\exp(-6D_\perp t) \tag{9}$$

$D_\perp$, is the rotational diffusion coefficient perpendicular to the main symmetry axis.) The measured rotational correlation times are plotted vs viscosity in Figure 8.

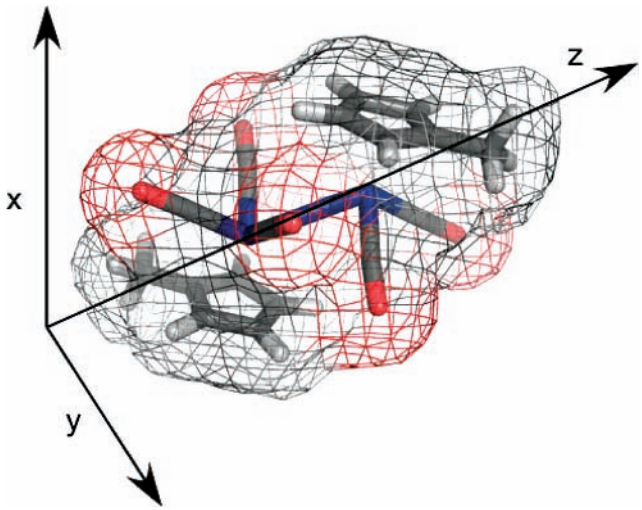

Figure 7. Representation of the shape of the *anti*-$[Cp'Mo(CO)_3]_2$ molecule with major symmetry axis ($z = 5.9$ Å) and nearly degenerate minor axes ($x \approx y = 2.7$ Å). The shape of the dimer is very nearly approximated as a prolate ellipsoid, and the main symmetry axis is nearly collinear with the chromophoric axis (Mo−Mo bond). The mesh is a representation of the molecular van der Waals radius.

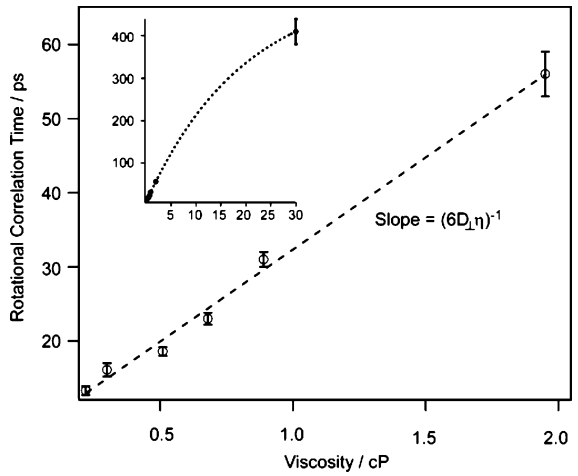

Figure 8. Rotational correlation time of $[Cp'Mo(CO)_3]_2$ vs viscosity. The dashed line represents a linear least squares fit to the data. The inset includes the data point for squalane ($\eta = 30$ cP), which displays a slight deviation from a linear viscosity/correlation time relationship. The dashed line in the inset is provided as a visual guide only. The rotational diffusion coefficient for the dimer was calculated with the exclusion of the squalane data point in order to generate a more appropriate estimate for the data set. The measured slope $(6D_\perp\eta)^{-1}$ is 2.5×10^{11} s cP^{-1}.

A linear relationship between solvent viscosity and rotational correlation time is taken as evidence of Stokes−Einstein−Debye (SED) behavior. For a spherical solute, SED predicts the rotational correlation time by hydrodynamic friction with the solvent (eq 10), where τ_{rot} is the rotational correlation time, D_r

$$\tau_{rot} = \frac{1}{6D_r} = \frac{V_M\eta}{k_BT} \tag{10}$$

is the rotational diffusion coefficient, V_M is the hydrodynamic volume of the solute, η is the solvent viscosity, k_B is Boltzmann's constant, and T is the absolute temperature. Because the SED equation treats the solvent as a viscous continuum, the relationship is considered to be quantitatively accurate only when applied to very large solutes. Improvements to the theory, including descriptions of nonspherical solutes and quantitative treatment of the solute/solvent boundary conditions, have improved the estimations obtained from SED. However, even with the appropriate corrections, SED can often generate correlation time estimates for small molecules that may be in error by an order of magnitude. Also, the calculations are very sensitive to small variations in the shape of the solute. For this reason, estimates for the rotational correlation time of the radical fragments were obtained by a simple transformation of the empirically measured dimer correlation times.

The empirically measured dimer correlation times are a measurement of $D_\perp$, the rotational diffusion coefficient perpendicular to the main symmetry axis. The determination of $D_\perp$ was obtained from the linear fit of the correlation time data (Figure 8), where the slope is given by $(6D_\perp\eta)^{-1}$. This can be used to estimate $D_\parallel$ (equivalent to the rotational diffusion coefficient of the radical) by considering the exact formulation for $D_\perp$ and $D_\parallel$ as a function of the axial ratio, ρ, for a symmetric ellipsoid.[59] Simplifying these expressions for the ratio $D_\parallel/D_\perp$ yields eq 11:

$$\frac{D_\parallel}{D_\perp} = \frac{(S-\rho)(1+\rho^2)}{S+\rho-2S\rho^2} \tag{11}$$

TABLE 2: Empirically Measured Rotational Correlation Times of $[Cp'Mo(CO)_3]_2$ and Calculated Rotational Correlation Times of $Cp'Mo(CO)_3$ in Various Hydrocarbon Solvents

solvent	viscosity/ cP	τ_{dim} dimer rotational correln time/ps	$\tau_{rad}Cp'Mo(CO)_3^\bullet$ rotational correln time[a]/ps
pentane	0.22	13.3 ± 0.6	2.9
hexane	0.3	16.1 ± 0.9	4.0
heptane	0.39	18.6 ± 0.6	5.1
octane	0.51	23.0 ± 0.8	6.7
methylcyclohexane	0.68	31 ± 1	9.0
cyclohexane	0.89	36 ± 1	11.7
1-propanol	1.95	56 ± 3	25.7
squalene	30	410 ± 30	NA

[a] Estimated radical correlation times defined as $\tau_{rad} = 1/(6D_\parallel)$ (see text).

where S is given by

$$S = \frac{1}{\sqrt{\rho^2-1}}\ln[\rho\sqrt{\rho^2-1}] \tag{12}$$

Inserting the axial ratio, ρ, of the $[Cp'Mo(CO)_3]_2$ molecule into eq 11 generates a $D_\parallel/D_\perp$ ratio of approximately 1.9. This value is used to generate the estimated radical correlation rates displayed in Table 2, where $\tau_{rad} = 1/(6D_\parallel)$.

The closest comparison to a literature value for the measured rates is the study by Hochstrasser and co-workers, who measured the rotational correlation time of several similar metal carbonyls, namely $[CpFe(CO)_2]_2$, $[CpNi(CO)]_2$, and $[Cp^*Fe(CO)_2]_2$ ($Cp^* = \eta^5$-C_5Me_5). The average correlation time of these molecules was about 30 ps in cyclohexane,[62] a value about one-third that predicted from SED calculations. This is a deviation that is roughly consistent with our measurements. It should be noted that this treatment assumes the radical intermediate has hydrodynamic properties similar to the closed-shell dimer species. If the radical intermediate has significant specific interactions with the solvent, the compound may be stickier and rotate more slowly than predicted by this estimation.

In summary of this section, the quantitative estimation of the radical fragment rotational rate leads to the following conclusions: (1) The rotation of the radical fragments within the cage is proportional to solvent viscosity as predicted from SED theory. (2) The time scale for radical rotation in common solvents is comparable to or longer than the cage lifetime. Note that the rotational correlation time is the period necessary for a solute to rotate through 1 rad, and hence this result suggests that the radicals undergo only some slight rotation during an average cage encounter period. Consequently, the evidence suggests that the recombination event is not strongly controlled by rotational diffusion.[63]

Conclusions

The major conclusion of this study is that the dynamics of solvent cage reactions in large molecular systems are surprisingly similar to the results seen in much smaller molecules; i.e., solvent caging is dominated by a single, brief, encounter period after which the fragments are likely separated by an intercalating solvent molecule. Our results show that this primary encounter period lasts approximately 5 ps in a wide range of solvents and that the recombination efficiency during this period is controlled by translational diffusion. An investigation of the rotational dynamics of the system led to the finding that rotational relaxation is more rapid than is predicted by the SED model. However, the measured rotational relaxation times are still

sufficiently long to negate the hypothesis that in-cage geminate recombination is controlled by radical rotation. These results may apply to a broad range of photolytic chemical reactions, and further research is being conducted to extend these observations to molecular systems of increased steric mass to determine their generality.

Acknowledgment. We thank the NSF for funding through NSF-CHE-0452004 and an NSF IGERT fellowship to A.B.O.

References and Notes

(1) Lorand, J. P. *Prog. Inorg. Chem.* **1972**, *17*, 207−325.
(2) Franck, J.; Rabinowitch, E. *Trans. Faraday. Soc.* **1934**, *30*, 120−131.
(3) Noyes, R. M. *J. Chem. Phys.* **1955**, *23*, 1982.
(4) Noyes, R. M. *J. Am. Chem. Soc.* **1955**, *77*, 2042−2045.
(5) Noyes, R. M. *J. Am. Chem. Soc.* **1956**, *78*, 5486−5490.
(6) Zimmerman, J.; Noyes, R. M. *J. Chem. Phys.* **1950**, *18*, 658−666.
(7) Lampe, F. W.; Noyes, R. M. *J. Am. Chem. Soc.* **1954**, *76*, 2140−2144.
(8) Booth, D.; Noyes, R. M. *J. Am. Chem. Soc.* **1960**, *82*, 1868−1872.
(9) Meadows, L. F.; Noyes, R. M. *J. Am. Chem. Soc.* **1960**, *82*, 1872−1876.
(10) Xu, X.; Yu, S. C.; Lingle, R., Jr.; Zhu, H.; Hopkins, J. B. *J. Chem. Phys.* **1991**, *95*, 2445−2457.
(11) Smith, D. E.; Harris, C. B. *J. Chem. Phys.* **1987**, *87*, 2709−2715.
(12) Schwartz, B. J.; King, J. C.; Harris, C. B. *Understanding Chem. React.* **1994**, *7*, 235−248.
(13) Schwartz, B. J.; King, J. C.; Zhang, J. Z.; Harris, C. B. *Chem. Phys. Lett.* **1993**, *203*, 503−508.
(14) Liu, Q.; Wang, J. K.; Zewail, A. H. *Nature (London)* **1993**, *364*, 427−430.
(15) Lienau, C.; Zewail, A. H. *J. Phys. Chem.* **1996**, *100*, 18629−18649.
(16) Scott, T. W.; Doubleday, C., Jr. *Chem. Phys. Lett.* **1991**, *178*, 9−18.
(17) Hyde, M. G.; Reid, G. D.; Beddard, G. S. *Chem. Phys. Lett.* **1992**, *190*, 130−134.
(18) Lenderink, E.; Duppen, K.; Wiersma, D. A. *Chem. Phys. Lett.* **1992**, *194*, 403−409.
(19) Scott, T. W.; Liu, S. N. *J. Phys. Chem.* **1989**, *93*, 1393−1396.
(20) Bultmann, T.; Ernsting, N. P. *J. Phys. Chem.* **1996**, *100*, 19417−19424.
(21) Lochschmidt, A.; Eilers-Koenig, N.; Heineking, N.; Ernsting, N. P. *J. Phys. Chem. A* **1999**, *103*, 1776−1784.
(22) Turro, N. J. *Abstracts of Papers*, 231st ACS National Meeting, Atlanta, GA, March 26−30, 2006; American Chemical Society: Washington, DC, 2006; ORGN-040.
(23) Sivaguru, J.; Saito, H.; Solomon, M. R.; Kaanumalle, L. S.; Poon, T.; Jockusch, S.; Adam, W.; Ramamurthy, V.; Inoue, Y.; Turro, N. J. *Photochem. Photobiol.* **2006**, *82*, 123−131.
(24) Poon, T.; Turro, N. J.; Chapman, J.; Lakshminarasimhan, P.; Lei, X.; Adam, W.; Bosio, S. G. *Org. Lett.* **2003**, *5*, 2025−2028.
(25) Turro, N. J.; Buchachenko, A. L.; Tarasov, V. F. *Acc. Chem. Res.* **1995**, *28*, 69−80.
(26) Zhang, J. Z.; Harris, C. B. *J. Chem. Phys.* **1991**, *95*, 4024−4032.
(27) Wrighton, M. S.; Ginley, D. S. *J. Am. Chem. Soc.* **1975**, *97*, 4246−4251.
(28) Meyer, T. J.; Caspar, J. V. *Chem. Rev.* **1985**, *85*, 187−218.
(29) Bitterwolf, T. E. *Coord. Chem. Rev.* **2001**, *211*, 235−254.
(30) Levenson, R. A.; Gray, H. B. *J. Am. Chem. Soc.* **1975**, *97*, 6042−6047.
(31) Scott, S. L.; Espenson, J. H.; Zhu, Z. *J. Am. Chem. Soc.* **1993**, *115*, 1789−1797.
(32) Yao, Q.; Bakac, A.; Espenson, J. H. *Organometallics* **1993**, *12*, 2010−2012.
(33) Peters, J.; George, M. W.; Turner, J. J. *Organometallics* **1995**, *14*, 1503−1506.
(34) Linehan, J. C.; Yonker, C. R.; Addleman, R. S.; Autrey, S. T.; Bays, J. T.; Bitterwolf, T. E.; Daschbach, J. L. *Organometallics* **2001**, *20*, 401−407.
(35) Hooker, R. H.; Mahmoud, K. A.; Rest, A. J. *J. Chem. Soc., Dalton Trans.* **1990**, 1231−1241.
(36) Baker, M. L.; Bloyce, P. E.; Campen, A. K.; Rest, A. J.; Bitterwolf, T. E. *J. Chem. Soc., Dalton Trans.* **1990**, 2825−2832.
(37) Hooker, R. H.; Mahmoud, K. A.; Rest, A. J. *J. Organomet. Chem.* **1983**, *254*, C25−C28.
(38) Mahmoud, K. A.; Rest, A. J.; Alt, H. *J. Chem. Soc., Dalton Trans.* **1984**, 187−197.
(39) Waldman, A.; Ruhman, S.; Shaik, S.; Sastry, G. N. *Chem. Phys. Lett.* **1994**, *230*, 110−116.
(40) Kim, S. K.; Pedersen, S.; Zewail, A. H. *Chem. Phys. Lett.* **1995**, *233*, 500−508.
(41) Owrutsky, J. C.; Baronavski, A. P. *J. Chem. Phys.* **1996**, *105*, 9864−9873.
(42) Yang, H.; Snee, P. T.; Kotz, K. T.; Payne, C. K.; Harris, C. B. *J. Am. Chem. Soc.* **2001**, *123*, 4204−4210.
(43) Manning, A. R.; Hackett, P.; Birdwhistell, R.; Soye, P. *Inorg. Synth.* **1990**, *28*, 148−50.
(44) Kafka, J. D.; Baer, T. *Opt. Lett.* **1987**, *12*, 401−403.
(45) Ziolek, M.; Lorenc, M.; Naskrecki, R. *Appl. Phys. B: Lasers Opt.* **2001**, *72*, 843−847.
(46) Rasmusson, M.; Tarnovsky, A. N.; Akesson, E.; Sundstrom, V. *Chem. Phys. Lett.* **2001**, *335*, 201−208.
(47) See, for example: Rice, S. A. In *Comprehensive Chemical Kinetics*; Bamford, C. H., Tipper, C. F. H., Compton, R. G., Eds.; Elsevier: Amsterdam, 1985; Vol. 25.
(48) Braden, D. A.; Parrack, E. E.; Tyler, D. R. *Coord. Chem. Rev.* **2001**, *211*, 279−294.
(49) Kiefer, H. R.; Traylor, T. G. *J. Am. Chem. Soc.* **1967**, *89*, 6667−6671.
(50) Kodama, S. *Bull. Chem. Soc. Jpn.* **1962**, *35*, 827−832.
(51) Pryor, W. A.; Smith, K. *J. Am. Chem. Soc.* **1970**, *92*, 5403−5412.
(52) Smith, W. F., Jr.; Eddy, K. L. *Tetrahedron* **1970**, *26*, 1255−1259.
(53) Owrutsky, J. C.; Raftery, D.; Hochstrasser, R. M. *Annu. Rev. Phys. Chem.* **1994**, *45*, 519−555.
(54) Joly, A. G.; Nelson, K. A. *Chem. Phys.* **1991**, *152*, 69−82.
(55) Steinhurst, D. A.; Baronavski, A. P.; Owrutsky, J. C. *Chem. Phys. Lett.* **2002**, *361*, 513−519.
(56) George, M. W.; Dougherty, T. P.; Heilweil, E. J. *J. Phys. Chem.* **1996**, *100*, 201−206.
(57) Harris, A. L.; Brown, J. K.; Harris, C. B. *Annu. Rev. Phys. Chem.* **1988**, *39*, 341−366.
(58) Elsaesser, T.; Kaiser, W. *Annu. Rev. Phys. Chem.* **1991**, *42*, 83−107.
(59) Fleming, G. R. *Chemical Applications of Ultrafast Spectroscopy*; International Series of Monographs on Chemistry 13; Oxford University Press: Oxford, 1986.
(60) Adams, R. D.; Collins, D. M.; Cotton, F. A. *Inorg. Chem.* **1974**, *13*, 1086−1090.
(61) Adams, R. D.; Cotton, F. A. *Inorg. Chim. Acta* **1973**, *7*, 153−156.
(62) Lian, T.; Locke, B.; Iannone, M.; Hochstrasser, R. M. *Springer Proc. Phys.* **1992**, *68*, 93−95.
(63) Beddard, G. S.; Masters, A. J. *Chem. Phys. Lett.* **1992**, *188*, 513−519.